Direct numerical simulation of salt sheets and turbulence in a double-diffusive shear layer

Satoshi Kimura[1] and William Smyth[1]

Received 5 September 2007; accepted 9 October 2007; published 15 November 2007.

[1] We describe three-dimensional direct numerical simulations (DNS) of double-diffusively stratified flow interacting with inflectional shear. The extreme difference in diffusivity (and thus minimum length scale) between heat, salt and momentum in seawater is replicated for the first time in a three-dimensional simulation. The primary instability generates salt sheets, which are oriented parallel to the direction of the sheared background flow. Subsequently, two distinct mechanisms of secondary instability combine to lead the flow to a turbulent state. In this state, the effective saline diffusivity is smaller than that calculated by previous investigators for the unsheared case. The Schmidt number is much smaller than unity, indicating that salt sheets are less effective at transporting momentum than is often assumed. **Citation:** Kimura, S., and W. Smyth (2007), Direct numerical simulation of salt sheets and turbulence in a double-diffusive shear layer, *Geophys. Res. Lett.*, *34*, L21610, doi:10.1029/2007GL031935.

1. Introduction

[2] Stratification in the ocean is determined by two components, temperature and salinity. Gravitationally stable stratification (i.e. light over heavy) can be maintained even though one of the components is unstably distributed. If salt is unstably distributed, salt fingers may grow [e.g., *Kunze*, 2003]. In a large portion of the subtropical ocean, evaporation exceeds precipitation at the same time heating exceeds cooling. Consequently, warm salty water is produced on the surface that stays above cooler, fresher water [*Schmitt*, 2003].

[3] In a quiescent environment, double-diffusive instability creates a rich variety of salt finger planforms [*Schmitt*, 1994]. In the presence of a sheared, horizontal ambient current, the preferred mode takes the form of vertical sheets aligned parallel to the flow [*Linden*, 1974]. These structures are now called salt sheets. In the ocean, salt fingering instability may organize the water column into a thermohaline staircase [*Radko*, 2003; *Schmitt*, 2003]. In this case, ubiquitous background shear tends to be focused at depths where double-diffusive instability is strong [*Gregg and Sanford*, 1987]. It is therefore anticipated that the resulting instability will have the form of salt sheets. Another example is thermohaline interleaving, in which interleaving motions create a shear across salt fingering layers [e.g. *Mueller et al.*, 2007].

[4] Here, we use three-dimensional (3D) direct numerical simulation (DNS) to investigate the transition to turbulence in a bounded fluid with non-uniform vertical gradients of salinity, temperature and horizontal current. Resolving the spatial scales associated with the slowly diffusing scalar, salinity, is a computational grand challenge. Our computation employs the realistic value of saline diffusivity in 3D DNS for the first time.

[5] Section 2 discusses the DNS model and initial conditions. Section 3 discusses the sequence of instabilities that leads to turbulence. The turbulent state is described in section 4, and conclusions are summarized in section 5.

2. Methodology

[6] We assume that the total buoyancy b is the sum of thermal and saline buoyancy components (b_T and b_S, resp.), each of which is governed by an advection-diffusion equation:

$$b = b_T + b_S; \quad \frac{Db_T}{Dt} = \kappa_T \nabla^2 b_T; \quad \frac{Db_S}{Dt} = \kappa_S \nabla^2 b_S. \tag{1}$$

$D/Dt = \partial/\partial t + \vec{u} \cdot \vec{\nabla}$ is the material derivative. The velocity field $\vec{u}(x, y, z, t) = \{u, v, w\}$ is measured in a nonrotating, Cartesian coordinate system $\{x, y, z\}$. We neglect inertial effects of density variations in accordance with the incompressible Boussinesq approximation:

$$\frac{D\vec{u}}{Dt} = -\nabla\pi + b\hat{k} + \nu\nabla^2\vec{u}; \quad \nabla \cdot \vec{u} = 0. \tag{2}$$

The variable π represents the pressure scaled by the characteristic density ρ_0, and $\hat{k}$ is the vertical unit vector. The total buoyancy is defined as $b = -g(\rho - \rho_0)/\rho_0$, where g is the acceleration due to gravity. Kinematic viscosity and thermal and saline diffusivities are denoted by ν, κ_T and κ_S, respectively.

[7] Boundary conditions are periodic in the horizontal, with periodicity intervals L_x and L_y in the streamwise (x) and spanwise (y) directions, respectively. Upper and lower boundaries, located at $z = 0$ and $z = L_z$, are impermeable ($w = 0$), stress-free ($\partial u/\partial z = \partial v/\partial z = 0$) and insulating with respect to both heat and salt ($\partial b_T/\partial z = \partial b_S/\partial z = 0$).

[8] For the experiments reported here, initial profiles were chosen to represent a stratified shear layer:

$$\frac{u}{\Delta u} = \frac{b_T}{\Delta B_T} = \frac{b_S}{\Delta B_S} = \tanh\left(\frac{z - \frac{L_z}{2}}{h}\right) \tag{3}$$

Here, Δu is the half-change of background velocity across a transition layer of half-depth h. ΔB_T and ΔB_S are the half-changes in thermal and saline buoyancy, respectively. The half-change in total buoyancy is then $\Delta B = \Delta B_T + \Delta B_S$.

[1]College of Oceanic and Atmospheric Sciences, Oregon State University, Corvallis, Oregon, USA.

0094-8276/07/2007GL031935$05.00

[9] The primary instability was seeded by adding an initial disturbance proportional to the fastest growing mode of linear theory [*Smyth and Kimura*, 2007], with amplitude chosen so that the maximum vertical parcel displacement was $0.02h_0$. To seed secondary instabilities the initial perturbation was supplemented with a random velocity field with maximum amplitude $0.01\Delta u$.

[10] Relevant parameter values for the three cases discussed here are given in Table 1 along with observed values. The differences in molecular diffusivity between heat, salt and momentum are described by the Prandtl number $Pr = \nu/\kappa_T$ and the diffusivity ratio $\tau = \kappa_S/\kappa_T$. In salt water, these ratios are far from unity, a circumstance that poses extreme challenges for numerical simulation as it leads to a wide range of spatial scales that must be resolved. The Prandtl number was set to 7, a typical value for water at oceanic temperatures. Given that the smallest scale of a scalar field is roughly proportional to the square root of its diffusivity, temperature is expected to vary on scales smaller than those of velocity by a factor $\sqrt{7} = 2.6$. The diffusivity ratio τ for salt water is about 0.01, so that salinity fluctuates on scales as small as a factor of ten below the smallest temperature scale. In previous DNS of salt water, this extreme difference in scales has required that τ be artificially increased [e.g., *Stern et al.*, 2001; *Gargett et al.*, 2003; *Smyth et al.*, 2005]. Thanks to advances in computer power, it is now possible to use the realistic value. Here we compare three simulations using $\tau = 0.01$ and higher values.

[11] The density ratio $R_\rho = -\Delta B_T/\Delta B_S$ was set to 1.6. The bulk (minimum) Richardson number $Ri = \Delta Bh/\Delta u^2$ was given the value 2. These choices ensure that double diffusive modes grow and are not overwhelmed by inflectional shear instabilities [*Smyth and Kimura*, 2007].

[12] A Reynolds number relevant for the initial growth of salt sheets in a sheared environment is constructed using the wavelength λ_{fg} of the fastest-growing salt sheet mode and the maximum background shear $S = \Delta u/h$: $Re_\lambda = \lambda_{fg}^2 S/\nu$. The wavelength is the same as that for salt fingers: $\lambda_{fg} = 2\pi(\nu\kappa_T h/\Delta B)^{1/4}$ [e.g., *Smyth and Kimura*, 2007]. Our value is the same as the observed value: $\lambda_{fg} = 0.046$m. This gives $Re_\lambda = 11$, which is at the high end of the observed range (Table 1).

[13] The spanwise periodicity interval L_y was chosen to accommodate two wavelengths of the fastest-growing primary instability. The appropriate value for L_x is not well known a priori, as it is determined by the streamwise wavelengths of the secondary instabilities whose presence is reported here for the first time. For the $\tau = 0.01$ and $\tau = 0.04$ cases, we set L_x to 8 m, which in retrospect is probably larger than necessary. For the $\tau = 0.16$ cases, we used the smaller value $L_x = 1$ m. Further research is needed to constrain this length scale more precisely.

[14] The numerical code used to solve (1)–(2) is described by *Winters et al.* [2004] with modifications as discussed by *Smyth et al.* [2005]. The slowly diffusing scalar, salinity, is resolved on a fine grid with spacing equal to one half the spacing used to resolve the other fields. A fit to the results of *Stern et al.* [2001] for 2D salt fingers suggests a fine grid spacing $\Delta = 0.15\ \lambda_{fg}\tau^{1/2}$ in the y and z directions. We have found that this choice gives adequate resolution of the salinity field. Because gradients are much gentler in the x direction, the corresponding grid increment is doubled. The remaining fields are computed on the coarse grid, but even so are extremely well-resolved.

3. The Transition to Turbulence

[15] Figure 1 shows the salinity field at selected times during DNS1. Figure 1a shows the primary "salt sheet" instability. Rising sheets of cool, fresh water (shown in red and yellow) alternate with sinking sheets of warm, salty water (blue and purple). The computational domain accommodates two wavelengths of the instability.

[16] When the salt sheets reach sufficiently large amplitude (Figure 1b), they exhibit two distinct secondary instabilities, which we will refer to as the "sheet" and "tip" instabilities. The sheet instability appears as a vertically-quasiperiodic buckling motion whose amplitude is largest at the center of the transition layer. The vertical wavelength is $\approx 1.8\lambda_{fg}$, consistent with that computed by *Stern and Simeonov* [2005] for unsheared two-dimensional salt fingers. Buckling regions show a slight tilt in the x-direction. The tip instability is focused at the tips of the salt sheets and shows rapid, quasiperiodic fluctuations in the x direction. Both instabilities are strongly modified as they reach large amplitude (Figure 1c). The sheet instability breaks down into turbulent motions that show the influences of both double-diffusive convection and the mean shear. The tip instability launches convective plumes into the upper and lower homogenous regions, where the influence of the mean shear is much weaker. The result is a complex, chaotic flow that we refer to as "double-diffusive turbulence". A statistical description of double diffusive turbulence is given in section 4.

[17] An alternative view of the transition process is gained via the instantaneous exponential growth rate for the velocity perturbation $\vec{u}'(x, y, z, t) = \vec{u}(x, y, z, t) - \overline{\vec{u}}(z, t)$, where the overbar indicates the horizontal average. Exponential growth rates for the velocity perturbation components are defined as

$$\sigma_u = \frac{1}{2}\frac{d}{dt}\ln\langle\overline{u'^2}\rangle; \quad \sigma_v = \frac{1}{2}\frac{d}{dt}\ln\langle\overline{v'^2}\rangle; \quad \sigma_w = \frac{1}{2}\frac{d}{dt}\ln\langle\overline{w'^2}\rangle. \quad (4)$$

Angle brackets denote an average over the vertical domain $0 \le z \le L_z$.

[18] Evolution of the growth rates for each of the three cases is shown in Figure 2. In each case, the initial perturbations adjust quickly to a state in which all three components of the perturbation kinetic energy grow at a common, nearly steady rate indicative of an exponentially-growing normal mode instability, i.e. salt sheets. The manifestation of this instability in the particular case of vertically localized stratification and shear is described by *Smyth and Kimura* [2007]. The growth rate evident in Figure 2 corresponds well with that calculated via linear stability analysis (indicated by thin, solid lines).

[19] After a period of slowly declining growth, each case exhibits a rapid increase in spanwise kinetic energy (thick, solid curves in Figure 2), followed by a similar period of increasing streamwise fluctuations (dash-dotted curves in Figure 2). Close inspection shows that these growth periods coincide with the emergence of the sheet and tip instabilities, respectively. In each simulation, the growth rates

Table 1. Typical Values of Non-Dimensional Parameters in the Ocean and in Our DNS Runs[a]

	DNS1	DNS2	DNS3	Ocean
Pr	7	7	7	7
τ	0.01	0.04	0.16	0.01
R_ρ	1.6	1.6	1.6	1.70 ± 0.15
Ri	2	2	2	3 ± 2
λ_{fg}[m]	0.046	0.046	0.046	0.046 ± 0.006
Re_λ	11	11	11	8 ± 3
L_x[m]	8	8	1	
L_y[m]	0.09	0.09	0.09	
L_z[m]	1.9	1.9	1.9	
N_x	6144	3072	384	
N_y	144	144	40	
N_z	3072	1536	768	

[a]Diffusivities are standard values for salt water at 20 °C. Observed values of R_ρ, Ri, λ_{fg} and Re_λ are taken from *Gregg and Sanford* [1987] as summarized in their figure 3. Nine sheared, double-diffusive interfaces were observed. The range quoted is the mean plus or minus one standard deviation.

associated with the two secondary instabilities subside, and the flow evolves to a state where the growth rates fluctuate around zero.

[20] The dependence of the transition process upon the diffusivity ratio τ may be assessed via comparison of Figures 2a–2c. The maximum growth rate of the primary instability is nearly independent of τ, as is expected from the results of linear stability analysis [e.g., *Smyth and Kimura*, 2007]. In contrast, the secondary instabilities show a clear dependence on τ: the sequence of events is unchanged, but the time scale and instability strength varies. When τ is increased to 0.16, secondary instabilities appear much later, and the maximum growth rates of both instabilities are significantly reduced. At $\tau = 0.04$, the evolution is much closer to the $\tau = 0.01$ case, with only a slight delay and weakening of the secondary instabilities.

4. Double-Diffusive Turbulence

[21] The secondary instabilities discussed above cause the flow to evolve to a complex state, in which chaotic motions are driven by the combination of double-diffusive convection and ambient shear, and which we refer to here as double-diffusive turbulence (Figure 1c). In this section, properties of double-diffusive turbulence are described in terms of various combinations of vertical fluxes and associated diffusivities.

[22] The central region is expected to correspond best to the previous experiments of *Stern et al.* [2001], which focused on vertically-homogenous salt fingers. Effective diffusivities for saline buoyancy and momentum in that region are defined via standard flux-gradient parameterizations:

$$K_S = -\overline{w'b'_S}\Big/\frac{\partial \overline{B_S}}{\partial z}, \quad K_U = -\overline{u'w'}\Big/\frac{\partial \overline{U}}{\partial z}. \tag{5}$$

The fluxes are computed at the midplane $z = L_z/2$. The gradients are defined by fitting the saline buoyancy profile to a hyperbolic tangent profile like (3), but with adjustable thickness. More specifically, we fit $\overline{b_S}$ to a function $f = a\ \tanh[(z - Lz/2)/b]$ by minimizing the weighted error $E = \langle(\overline{b_S} - f)^2(z - L_z/2)^2\rangle$. The weighting emphasizes the outer regions of the profile. The central gradient is then equal to a/b. This choice captures the slow diffusion of the transition layer but is insensitive to more rapid fluctuations due to the growth of salt sheets.

[23] The effective saline diffusivity for unsheared 3D salt fingers for $\tau = 0.01$ was estimated by *Stern et al.* [2001]. They calculated the ratio of 2D to 3D fluxes using numerically accessible values of τ, then multiplied that ratio onto the directly computed fluxes for 2D fingers with $\tau = 0.01$. The resulting estimate of the effective saline diffusivity is $2.4 \times 10^{-5}\ m^2/s$, as shown by the triangle in Figure 3a. Also shown is the smaller value computed by Stern et al. for $\tau = 0.17$.

[24] In our DNS experiments, K_S starts off small, then grows exponentially with the growth of the primary instability. After reaching a maximum at the onset of secondary instability, K_S drops rapidly, then settles in to a state of slow decay modulated by faster fluctuations. In this late stage, K_S seems to be largely independent of τ.

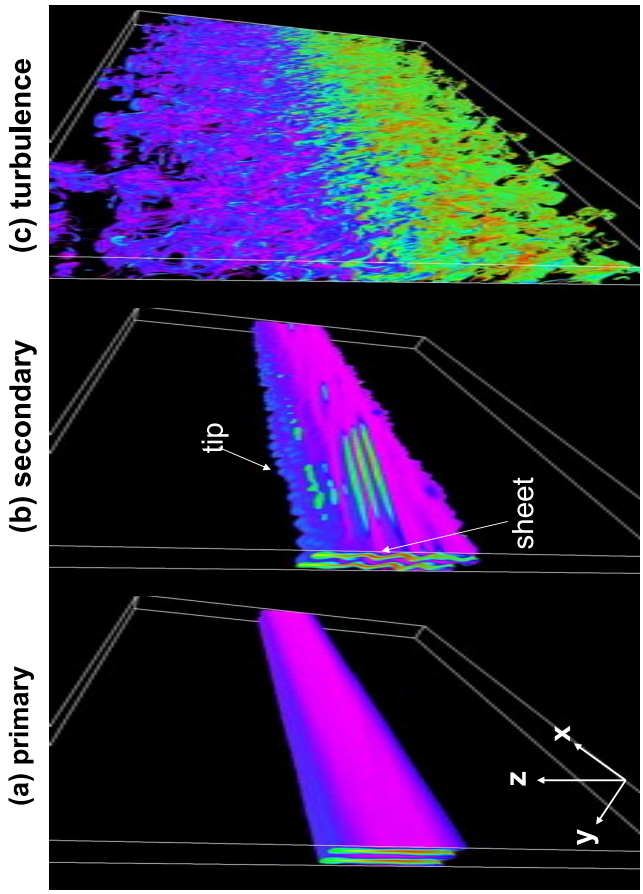

Figure 1. Evolution of the salinity field for DNS1: (a) $t = 2944s$, (b) $t = 3362s$, and (c) $t = 5109s$. Homogeneous regions above and below the transition layer are rendered transparent. Within the transition layer, the highest salinities are shown in purple and blue; the lowest in red and yellow. Only half of the streamwise (x) domain extent is shown. Labels in Figure 1b indicate two distinct mechanisms of secondary instability as discussed in the text.

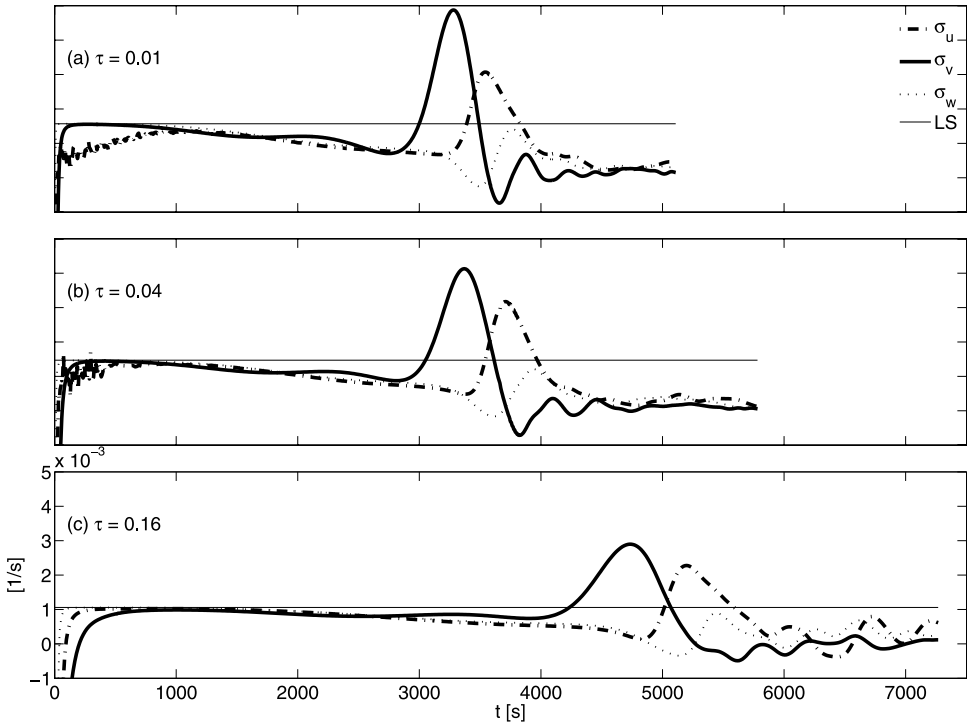

Figure 2. Growth rates as defined in equation (4). The LS line indicates the growth rate calculated from linear stability analysis. (a) DNS1, (b) DNS2, and (c) DNS3.

[25] The result is not consistent with the result of *Stern et al.* [2001], who found significant dependence on τ as shown by the symbols in Figure 3a. Our values of K_S are generally smaller than those of Stern et al., a difference that may be attributable to the effects of the mean shear. The difference may also be due to the difference in boundary conditions and initial profiles of thermal and saline buoyancy components. Stern et al. used periodic boundary conditions in the vertical coordinate where we used rigid boundaries for vertical velocity and flux-free boundaries for other variables. Our thermal and saline buoyancy component profiles had localized vertical gradients where Stern et al. used

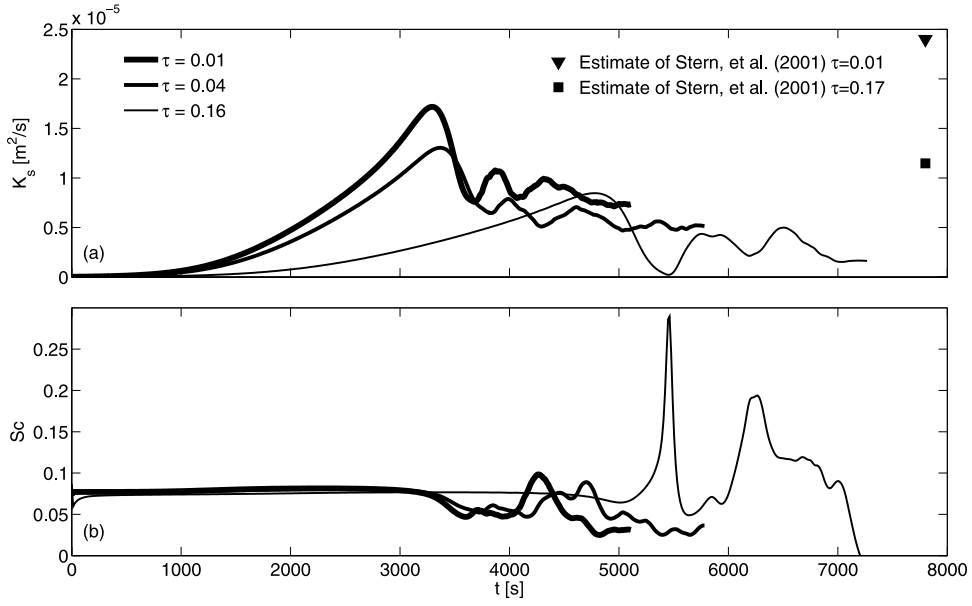

Figure 3. (a) Effective saline diffusivity. (b) Schmidt number. Thick, medium and thin curves correspond to cases DNS1, DNS2 and DNS3, respectively.

uniform vertical gradients. The decay of K_S may be due to the increasing thickness of the transition layer in our experiments.

[26] The Schmidt number, $Sc = K_U/K_S$, plays an important role in governing the thickness of thermohaline interleaving layers [*Toole and Georgi*, 1981; *Mueller et al.*, 2007; *Walsh and Ruddick*, 1995]. The Schmidt number is often chosen to be greater than one in order to obtain interleaving layers of realistic thickness [e.g. *Smyth*, 2007]. *Ruddick* [1985] [see also *Ruddick et al.*, 1989] suggested that transfer of momentum by salt fingers is negligible, since salt fingers rapidly lose their momentum deficits via lateral diffusion.

[27] *Smyth and Kimura* [2007] demonstrate that *Sc* is order one or less in the linear regime. Our results confirm that *Sc* is less than order one in the non-linear regime (Figure 3b). In fact, *Sc* drops from the linear value $\sim$0.08 to values that are generally even smaller with the onset of nonlinearity. In the later stages of flow evolution, *Sc* fluctuates considerably, but remains $\ll$1.

5. Conclusions

[28] We have investigated DNS of salt sheets in double-diffusive stratified layer and computed turbulence statistics in the non-linear regime. Our main findings are follows.

[29] 1. Primary instability generates salt sheets in accordance with *Linden* [1974] and *Smyth and Kimura* [2007]. Secondary instability is via two distinct mechanisms. The sheet mode introduces motion in the spanwise direction. Subsequently, fluctuating motion in the streamwise direction is amplified via the tip mode.

[30] 2. Increasing τ above the realistic value 0.01 decreases the peak values of spanwise and streamwise kinetic energy growth rates and causes secondary instabilities to evolve on a slower time scale.

[31] 3. K_S increases exponentially until the onset of secondary instability and decays rapidly afterwards. After the decay period, the flow attains a molecular diffusivity-independent state in which K_S is significantly lower than the value estimated for the unsheared cases [*Stern et al.*, 2001].

[32] 4. The transfer of momentum is much less efficient in sheared salt fingers than is often assumed, i.e. the Schmidt number is less than order one in the non-linear regime. This suggests that the increase in the layer thickness of thermohaline intrusions is not purely due to momentum transfer by double diffusive instabilities.

[33] In the future, we will perform explicit stability analyses to examine the mechanisms of the sheet and tip instabilities. Further DNS experiments will quantify the effects of Richardson number and R_ρ on transition phenomena and turbulence statistics. Mean shear may be affected by variety of "external" forces. In some cases, shear is maintained by an external forcing such as wind. The mean flow may also change direction periodically due to tides and other internal waves. The experiments presented here do not involve any external forcing. Future studies may include the effects of external forcing by adding an appropriate forcing term to (2).

[34] **Acknowledgments.** We gratefully acknowledge useful discussions with J. Simeonov, T. Radko, B. Ruddick and W. Merryfield. This work was supported by the National Science Foundation under grant 0453140. Computer time was provided via a Breakthrough Science (BTS) allocation at the National Center for Atmospheric Research. Color graphics were produced by VAPOR (www.vapor.ucar.edu). We are grateful for the help of Alan Norton in generating flow visualizations.

References

Gargett, A., W. Merryfield, and G. Holloway (2003), Direct numerical simulation of differential scalar diffusion in three-dimensional stratified turbulence, *J. Phys. Oceanogr.*, *33*, 1758–1782.

Gregg, M. C., and T. Sanford (1987), Shear and turbulence in thermohaline staircases, *Deep Sea Res.*, *34*, 1689–1696.

Kunze, E. (2003), A review of oceanic salt fingering theory, *Prog. Oceanogr.*, *56*, 399–417.

Linden, P. (1974), Salt fingers in a steady shear flow, *Geophys. Fluid Dyn.*, *6*, 1–27.

Mueller, R. D., W. D. Smyth, and B. R. Ruddick (2007), Shear and convective turbulence in a model of thermohaline intrusions, *J. Phys. Oceanogr.*, *37*, 2534–2549.

Radko, T. (2003), A mechanism for layer formation in a double diffusive fluid, *J. Fluid Mech.*, *497*, 365–380.

Ruddick, B. R. (1985), Momentum transport in thermohaline staircases, *J. Geopys. Res.*, *90*, 895–902.

Ruddick, B., R. W. Griffiths, and G. Symonds (1989), Frictional stress at a sheared double-diffusive interface, *J. Geophys. Res.*, *94*, 18,161–18,173.

Schmitt, R. W. (1994), Triangular and asymmetric salt fingers, *J. Phys. Oceanogr.*, *24*, 855–860.

Schmitt, R. (2003), Observational and laboratory insights into salt finger convection, *Prog. Oceanogr.*, *56*, 419–433.

Smyth, W. (2007), Instabilities of a baroclinic, double diffusive frontal zone, *J. Phys. Oceanogr.* (in press).

Smyth, W., and S. Kimura (2007), Instability and diapycnal momentum transport in a double-diffusive stratified shear layer, *J. Phys. Oceanogr.*, *37*, 1551–1565.

Smyth, W., J. Nash, and J. Moum (2005), Differential diffusion in breaking Kelvin-Helmholtz billows, *J. Phys. Oceanogr.*, *35*, 1004–1022.

Stern, M., T. Radko, and J. Simeonov (2001), Salt fingers in an unbounded thermocline, *J. Mar. Res.*, *59*, 355–390.

Stern, M., and J. Simeonov (2005), The secondary instability of salt fingers, *J. Fluid Mech.*, *533*, 361–380.

Toole, J., and D. Georgi (1981), On the dynamics of double diffusively driven intrusions, *Prog. Oceanogr.*, *10*, 123–145.

Walsh, D., and B. Ruddick (1995), Double diffusive interleaving: The effect of a nonconstant diffusivities, *J. Phys. Oceanogr.*, *25*, 348–358.

Winters, K., J. MacKinnon, and B. Mills (2004), A spectral model for process studies of rotating, density-stratified flows, *J. Atmos. Oceanic Technol.*, *21*(1), 69–94.

S. Kimura and W. Smyth, College of Oceanic and Atmospheric Sciences, Oregon State University, Ocean Admin Bldg, Corvallis, OR 97331, USA. (skimura@coas.oregonstate.edu)